

1
2
3
4
5
6
7
8
9
10
11
12
13
14
15
16
17
18
19
20
21
22
23
24
25
26
27
28
29
30
31
32
33
34
35
36
37
38
39
40
41
42
43
44
45
46

1

An Introduction to Cavity Ring-Down Spectroscopy

Kevin K. Lehmann¹, Giel Berden² and Richard Engeln³

¹Department of Chemistry, University of Virginia, USA

²FOM Institute for Plasma Physics 'Rijnhuizen', Nieuwegein, The Netherlands

³Department of Applied Physics, Eindhoven University of Technology, The Netherlands

1.1 Introduction

Spectroscopy, the study of the interaction of light (electromagnetic radiation) and matter, is the most ubiquitous and precise method available to the physical scientist. Especially for isolated atoms, molecules, and small clusters, it has no peer. It is used to elucidate the structure and dynamics of quantum systems from atomic nuclei to natural proteins. Essentially everything we know about the universe beyond the domain that humans and their instruments can physically touch, comes from spectroscopy. Without it, astronomy would be no more than stamp collecting. While a mature field, spectroscopy is periodically reborn by the development of new tools that open up new vistas, such as under-explored regions of the spectrum, dramatic improvements in resolution, or in sensitivity. Almost always, these are initially unexpected and have been developed to address some specific problem. However, truly seminal work inspires and leads to an explosion of new applications and with it advancement of methods. Nuclear magnetic resonance spectroscopy is the epitome of this experience.

This book is devoted to Cavity Ring-Down Spectroscopy (CRDS). Like most new methods in science, CRDS grew out of an advance in technology, in this case the dramatic improvement in the reflectivity of the best dielectric mirrors, which in turn was made

2 Cavity Ring-Down Spectroscopy: Techniques and Applications

1 possible by the development of the ion sputtering method for forming thin films. As mirror
2 reflectivity, R , grew ever closer to unity (i.e. all the light reflected) it became an increasing
3 challenge to measure that reflectivity since one could not, in practice, simply measure
4 the very small light intensity difference before and after reflection from the mirror.
5 One could easily measure the transmission of the mirror, T , but some light is also lost
6 to absorption and scattering in the dielectric mirrors, which are made from a large number of
7 thin layers of material with alternating index of refraction. It was recognized that one
8 could build a stable optical resonator from a pair of such mirrors and that the storage time of
9 light injected into such a cavity would be inversely proportional to the total loss per
10 reflection, i.e. $1 - R$. Particularly relevant for the development of CRDS was the work of
11 Anderson, Frisch, and Masser [1]. They energized the optical cavity with a laser and then
12 rapidly turned it off and observed the delay of intracavity light intensity by the decay of the
13 light transmitted through one of the mirrors. This intensity decayed exponentially in time
14 with a rate, $k = (1 - R) c/L$, where c is the speed of light and L is the distance between the
15 mirrors. The inverse of k is the cavity 'ring-down time', τ , which gives the mean time that
16 any photon will survive inside the cavity. $L_{\text{eff}} = \tau c = L/(1 - R)$ gives the mean distance
17 that light travels in the cavity.

18 It is useful to give some numbers for the reader to get a feeling for the size of things.
19 Rempe *et al.* [2] reported on a pair of mirrors that gave a decay time of $8 \mu\text{s}$ for a cavity
20 with $L = 4.0 \text{ mm}$, when the cavity was excited at 850 nm , from which they deduced
21 a loss of 1.6 ppm per mirror reflection. If these same mirrors were separated by 1.6 m
22 (still fitting on most optical tables) the L_{eff} would equal 1000 km ! These are the highest
23 reflectivity mirrors that the authors are aware of but, today, mirrors with less than 100 ppm
24 loss are available throughout the visible and near-IR. Low loss optical cavities are central
25 in many recent technical and scientific advances, including laser-based gyroscopes and
26 laser-based gravity wave detectors. Bilger *et al.* [3] have analyzed the fundamental
27 limits of dielectric mirror reflectivity and predict that mirrors with as low as 1 part in
28 10^9 should be attainable. Such mirrors can be viewed as one-dimensional photonic band
29 gap crystals, i.e. light within a certain band cannot propagate in the direction normal to the
30 layers. The optics text by Fowles [4] provides an introductory treatment of the theory of
31 dielectric mirrors.

32 Cavity ring-down as a spectroscopic tool began with a paper published by O'Keefe
33 and Deacon in 1988 [5] in which they showed that an instrument that had been constructed
34 to measure mirror reflectivity could be used to measure faint visible absorptions of air due
35 to highly forbidden transitions of molecular oxygen. Two years later, O'Keefe and the
36 group of Richard Saykally began publishing a series of papers that used CRDS to detect
37 electronic transitions in small metal clusters [6], and CRDS began to be adopted by a
38 number of groups. The age of CRDS had begun. Paldus and Kachanov have given an
39 extended history of cavity enhanced spectroscopic methods [7].

40 Continuing to think about the Rempe mirrors, if there is a gas between these mirrors, then
41 any absorption or scattering loss of that gas will contribute with the mirror loss to the cavity
42 decay rate. If the gas has an absorption of only 1 ppm per pass (far below what could be
43 measured by direct absorption measurement), this would cause a 63% increase in the
44 total loss per pass and 38% decrease in the ring-down time. In typical CRDS experiments,
45 the standard error in the determination of the cavity decay time or rate is of the order of
46 $1-0.01 \%$. If we assume our noise in determination of the fractional cavity decay rate is

1 0.1 %, then a sample loss per pass of only 3 parts per billion (ppb) could be detected with a
 2 signal to noise ratio (S/N) of 2:1 in a single cavity decay.

3 This tremendous sensitivity to loss is the primary, though not only reason, that interest in
 4 CRDS has exploded in the past two decades, finding a broad range of applications, many of
 5 which are covered in this volume. It has also been extended and modified in many ways so
 6 that CRDS can now be considered as a family of related methods. In addition, many other
 7 ways of exploiting low loss optical cavities in spectroscopic applications, what may be
 8 considered the cousins of the CRDS methods, have been reported.

9
 10

11 1.2 Direct Absorption Spectroscopy

12

13 Direct absorption spectroscopy is a simple, noninvasive, *in situ* technique for obtaining
 14 information on the species in the gas, liquid or solid phase. From an absorption spectrum,
 15 quantitative absolute concentrations and absolute frequency-dependent cross-sections can
 16 be extracted. In a direct absorption experiment, the attenuation of light traveling through a
 17 sample is measured. The transmitted intensity follows the Beer–Lambert law

18

$$19 \quad I = I_0 \exp(-\alpha d) \quad (1.1)$$

20

21 where I_0 is the intensity of the incident light, d the length of the sample, and α the absorption
 22 coefficient of the sample. In case of the absorption being caused by a single species,
 23 $\alpha(\nu) = N\sigma(\nu)$ with N being the number density (molecules per unit volume) of the
 24 absorber, $\sigma(\nu)$ the absorption cross-section, and ν the frequency of the light. More
 25 generally, one must sum over all the absorption and scattering losses that contribute to $\alpha(\nu)$.

26 An example of a direct absorption set-up is shown in Figure 1.1. Here the light source is a
 27 tunable laser, and the sample, for example a gas, is contained in a cell. The laser light enters
 28 the cell via a window. The attenuated laser light exits the cell via a second window and the
 29

30

31

32

33

34

35

36

37

38

39

40

41

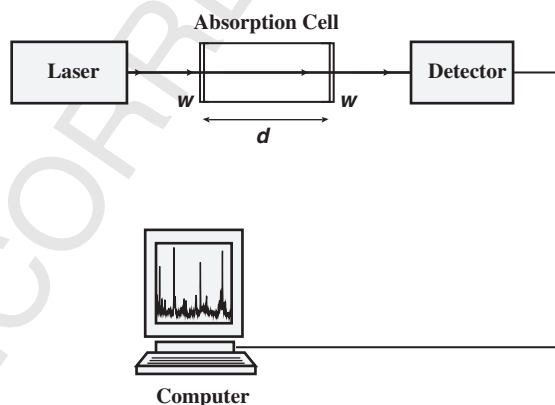
42

43

44

45

46



44 **Figure 1.1** Experimental set-up for single-pass direct absorption spectroscopy. The sample is
 45 contained in the absorption cell with length d . The transmission of the light through the cell is
 46 measured as a function of the wavelength (w is a window)

1 intensity of the light is measured with a suitable detector. By recording the intensity as
2 a function of wavelength, an absorption spectrum is obtained.

3 This so-called single pass absorption technique suffers from a low sensitivity that
4 limits its application in many research fields (e.g. trace gas detection). This low sensitivity
5 results from the fact that a small light attenuation has to be measured on top of a large
6 background signal that is proportional to the intensity of the light source. For stable light
7 sources, one can at best detect a change on the order 10^{-3} . Pulsed lasers, which cover a
8 broad wavelength range from the ultraviolet to the infrared, exhibit large pulse-to-pulse
9 intensity fluctuations, and are not well suited for single-path absorption experiments.

10 The sensitivity can be improved by using indirect absorption techniques, which are
11 based upon the measurement of an effect induced by the absorption of light rather than the
12 absorption of light itself. In the laser induced fluorescence (LIF) technique, molecules
13 absorb light and are electronically excited. The fluorescence, that is, the light emitted
14 when the molecules decay back to their ground state, is then measured. In principle, LIF is a
15 background free technique, but scattered light from the excitation laser can contribute to
16 noise. If there is a significant Stokes shift in the emission, a spectral filter can be used to
17 block most of the scattered light. One can also use time-gated detection to block most of the
18 remaining scattered light while still detecting much of the fluorescence in case the
19 fluorescence lifetime is longer than the exciting laser pulse. In favorable cases (when an
20 atom or molecule can sequentially absorb and emit many photons), single atoms or
21 molecules can be detected. Typically, LIF detection cannot be used for direct excitation
22 of vibrational transitions due to the low spontaneous emission rate ($\sim 1 \text{ s}^{-1}$) and the poorer
23 sensitivity of IR detectors. Furthermore, due to collisional quenching and increased
24 scattering, LIF is less suited to applications at high pressure. The same applies to excited
25 electronic states that have poor quantum yields for emission.

26 In the resonant enhanced multiphoton ionization (REMPI) technique, molecules are
27 ionized after absorption of two or more photons via intermediate energy levels of the
28 neutral molecule. REMPI is background free, and can be combined with mass-selection,
29 commonly by using the time-of-flight method. By using extraction fields, one can detect
30 essentially all of the generated ions. Despite its high sensitivity and selectivity, REMPI is
31 difficult to perform under atmospheric conditions. It also is difficult to use it to detect
32 vibrational transitions or excited electronic states that undergo rapid nonradiative decay.
33 Due to the multi-photon nature of REMPI detection, the absolute signal strength is highly
34 dependent on focusing and even the laser pulse shape, and this makes it very difficult to use
35 REMPI for quantitative measurements.

36 When the energy deposited in a molecule is not reemitted, collisional relaxation will
37 convert this energy into heat, and this will raise the temperature and pressure of the gas.
38 Thus, the absorption of an amplitude modulated light beam by a sample will lead to
39 production of a sound wave that can be detected. This photoacoustic (or optoacoustic) effect
40 was first investigated by Alexander Graham Bell, who by 1881 was already investigating
41 methods for optical communications. The amplitude of the generated sound is proportional
42 to the optical power absorbed by the sample. With tunable laser sources, the sound level
43 versus laser frequency is detected, which is known as Photoacoustic Spectroscopy (PAS).
44 PAS can be applied to solids, liquids, and gases, and is only sensitive to sample absorption,
45 not scattering losses. In many experiments, the sample is contained in an acoustic resonant
46 structure and the light is modulated at the resonance frequency, which enhances the signal

1 level [8]. The signal is proportional to the optical power on the sample, so high power lasers,
2 such as CO₂ lasers, are typically used for PAS of gases. Alternatively, the sample can be
3 placed inside a laser resonator cavity in order to increase the power on the sample. Since the
4 threshold sensitivity of the human ear, and the lowest noise microphones, is a pressure
5 increase of $\sim 10^{-9}$ bar, only a tiny heat power is required to produce a detectable sound
6 signal. Absorption sensitivities of $\sim 10^{-10}$ cm⁻¹ have been reported when high power
7 continuous wave lasers are used [9,10], comparable to the sensitivity limit of CRDS. The
8 sensitivity is much less when only low power lasers are available. Ambient noise and noise
9 generated by gas flow can also significantly reduce sensitivity. PAS instruments utilizing
10 quartz tuning forks have allowed improved environmental noise immunity and detection
11 of ~ 1 mm³ gas samples [11]. PAS requires sufficient pressure for collisional relaxation
12 and for efficient acoustic coupling to the microphone and thus sensitivity suffers at gas
13 pressures much below 1 bar. Because of the indirect detection, calibration samples or
14 components of the gas are required in order to obtain absolute absorption cross-sections
15 or concentrations. One of the present authors abandoned PAS for CRDS precisely because
16 of the difficulty in calibration of signal strength in the former.

17 A method related to PAS is thermal lensing spectroscopy [12]. This method exploits the
18 spatially dependent index of refraction of a sample induced by the heating created by
19 absorption of a focused laser. This makes the sample into a weak negative lens, which can be
20 monitored by the deflection or change in spot size of a continuous-wave probe laser that
21 passes through the same focus spot of the sample.

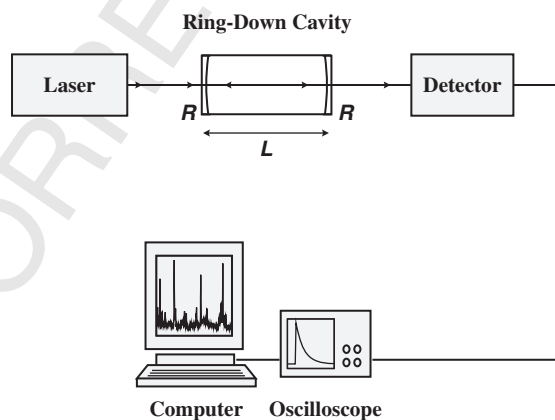
22 Although indirect absorption techniques have a spectacular sensitivity, they are not
23 self-calibrating; only a relative absorption coefficient is obtained. The attractive feature of
24 direct absorption spectroscopy is that it provides the absolute absorption coefficient in a
25 very simple way. The sensitivity of single-pass absorption spectroscopy can be increased by
26 increasing the path length through the sample (i.e., increasing d in Equation (1.1)). This can
27 be achieved with sophisticated multi-pass configurations, like for example, a White cell [13]
28 or a Herriott cell [14,15]. A multi-pass cell consists of two or more highly reflective mirrors.
29 Upon each reflection, light traverses the cell via a different optical path. With advanced
30 configurations, absorption path lengths of a few hundred meters can be achieved. However,
31 in these traditional multi-pass absorption cells, the individual passes of light must be
32 spatially separated. This leads to the need to use relatively large mirrors and sample
33 volumes. Also, even a very small overlap of light making different numbers of passes
34 through the cell leads to interference fringes and intensity noise in the transmitted light of
35 the cell, which often limits sensitivity. By rapid ($f_m \sim 100$ MHz) frequency modulation
36 of the laser, one can detect absorption at high frequency, above the excess intensity noise of
37 most lasers (though one still of course has shot noise). In principle, frequency modulation
38 should produce no amplitude signal on the detector unless the absorption or propagation
39 phase shift is different at the frequencies shifted $\pm f_m$ from the laser frequency, though in
40 practice real frequency modulators also introduce some residual amplitude modulation
41 as well. This detection method is known as frequency modulation (FM) spectroscopy,
42 and this allows sensitivity to sample absorption of $\sim 10^{-6}$ to be detected [16]. Combined
43 with path lengths of ~ 100 m obtainable with a multiple pass cell, one obtains absorption
44 coefficient sensitivity of $\sim 10^{-10}$ cm⁻¹. However, this sensitivity is only realized for
45 absorption features with a line width comparable to f_m and decreases for larger line widths
46 where we are effectively detecting the first or second derivative of the absorption versus

1 frequency (depending on whether one is detecting intensity modulation at f_m or $2f_m$).
 2 A comparison of FM spectroscopy and CRDS can be found in Chapter 6 and in the
 3 references [17,18].
 4 It can be imagined that spatially overlapping all of the passes in the cell dramatically
 5 reduces the probed sample volume. Further, since the different passes do not have to be
 6 spatially resolved, the number of passes of the sample is, in principle, only limited by the
 7 losses of the mirrors and sample, suggesting that sensitivity can be increased. However,
 8 the absorption cell will act as an optical resonator and will only transmit light in very narrow
 9 frequency intervals if the mirror reflectivity is high. Even tiny (\sim kHz) levels of laser
 10 frequency instability or mechanical jitter of the mirrors of picometers will lead to high noise
 11 in the transmitted cavity intensity if the highest reflectivity mirrors are used. Thus, direct
 12 absorption measurements using such cells would appear unpromising. However, by
 13 changing the focus to considering the cell as a storage vessel for light, the above-mentioned
 14 problems are overcome and much higher sensitivity to tiny levels of sample than was
 15 previously possible is achieved. This change to looking at light intensity as a function of
 16 time leads to cavity ring-down spectroscopy.

19 1.3 Basic Cavity Ring-Down Spectroscopy Set-Up

20
 21 Both because it was the first approach used for CRDS and because it is perhaps the
 22 simplest to understand, we will begin with a description of CRDS using a pulsed laser to
 23 excite the cavity. Figure 1.2 shows a typical pulsed CRDS set-up. It is largely representative
 24 of that used in all the early CRDS papers and is perhaps still the most commonly used
 25 method.

26 Light from a pulsed laser is focused into an optical cavity formed by two dielectric
 27 concave mirrors (or one flat and one curved mirror). The length of the cavity, L , and the



43 **Figure 1.2** Experimental set-up for cavity ring-down absorption spectroscopy. The sample
 44 is contained in the ring-down cavity with length L consisting of two mirrors with reflectivity R .
 45 The decay time of a light pulse trapped in the ring-down cavity is measured as a function of
 46 wavelength

1 radius of curvature of the mirrors should be chosen such that the cavity is optically stable
 2 (see Chapter 2). For example, for a 40-cm cavity with two identical mirrors, the radius of
 3 curvature of the mirrors must be greater than 20 cm in order to be stable. The mirrors are
 4 placed in adjustable mirror mounts that allow the mirrors to be tilted in order to align the
 5 cavity. See Section 10.3.6 of Chapter 10 for a procedure to align the ring-down cavity.

6 Light enters the cavity by transmission through one of the mirrors and light transmitted
 7 through the other mirror is used to monitor the intracavity light intensity as a function of
 8 time. Only a few ppm of the laser light enter the cavity, the rest being reflected. This modest
 9 amount of light (~ 1 nJ) entering the cavity experiences a small loss on each transmission
 10 of the cell and by mirror reflection, with a few parts per million of the energy transmitted
 11 out of each mirror on each cell round trip. The light transmitted by the back mirror is focused
 12 onto a photodetector, such as photomultiplier tube (PMT). Photodiodes can be used in
 13 spectral regions where PMTs are not available or for high signal-to-noise measurements,
 14 due to the excellent linearity of silicon photodiodes. The signal from the light detector is
 15 processed to extract the cavity decay rate, and from this the sample absorption coefficient.

16 In a simple picture, where the duration of the laser pulse width is shorter than the
 17 round-trip time of the pulse in the cavity, the detector will see a train of pulses (see
 18 Figure 1.3), each only slightly less intense than the previous one. The separation between
 19 adjacent pulses is equal to the round trip time $t_r = 2L/c$. The intensity of the pulses will
 20 decrease due to absorption by the species in the cavity and the losses at the mirrors.
 21 Let us calculate the intensity at the detector. A laser pulse with an intensity I_{laser} is injected
 22 into a cavity of length L . The two mirrors of the cavity are identical and have a reflectivity R
 23 and a transmission T . For ideal mirrors, without absorption or scattering losses, $T = 1 - R$.
 24 However, T equal to 0.1 – 0.5 times $1 - R$ is more typical for mirrors used in CRDS. After
 25 one pass through the cavity, the intensity of the first optical pulse at the detector is obtained
 26 from Beer–Lambert’s law (see Equation (1.1)):

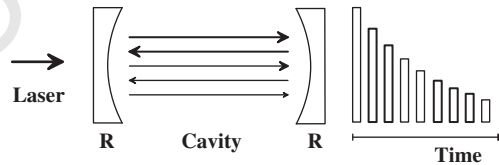
$$I_0 = I_{laser} T^2 \exp(-\alpha d) \tag{1.2}$$

27 where α is the frequency-dependent absorption coefficient of the medium in the cavity.
 28 Here it is assumed that the sample is only present over a length d of the cavity. The intensity
 29 of the second pulse is then given by:

$$I_1 = I_0 R^2 \exp(-2\alpha d) \tag{1.3}$$

30 where $R^2 \exp(-2\alpha d)$ is the loss due to the additional complete round trip through the cavity.
 31 Therefore, after n complete round trips, the pulse intensity behind the cavity will be

$$I_n = I_0 R^{2n} \exp(-2n\alpha d). \tag{1.4}$$



45 **Figure 1.3** Schematic of the description of the so-called ‘photon bullet model’ of the pulsed
 46 CRD technique

1 Because the loss per pass is small, it is easy to pick a bandwidth of the electronics such that
 2 the individual pulses circulating in the cavity are not seen, but do not significantly distort
 3 the cavity decay. In the previous formula this means that the discrete number of round trips
 4 n is replaced by the continuous parameter of time, $t = n \times 2L/c$. Furthermore, R^{2n} can be
 5 written as $\exp(2n \ln R)$, which leads to

$$6 \quad I(t) = I_0 \exp\left(\frac{tc}{L} (\ln R - \alpha d)\right). \quad (1.5)$$

8 Since the mirrors used in cavity ring-down spectroscopy have a reflectivity R close to 1,
 9 $\ln R \approx -(1-R)$, this can be rewritten as

$$11 \quad I(t) = I_0 \exp\left(-\frac{tc}{L} (1-R + \alpha d)\right). \quad (1.6)$$

13 The $1/e$ decay time of this exponentially decaying light intensity is called the ring down
 14 time τ and is defined as

$$16 \quad \tau = \frac{L}{c(1-R + \alpha d)}. \quad (1.7)$$

18 As discussed already in Section 1.2, in general one should sum over all light-scattering and
 19 light-absorbing species that contribute to $\alpha(\nu)$. Furthermore, it should be realized that the
 20 reflectivity of the mirrors depends on the frequency as well. Therefore, a more general
 21 relationship for the ring-down time is given by:

$$23 \quad \tau(\nu) = \frac{L}{c \left[1 - R(\nu) + \sum_i \sigma_i(\nu) \int_0^d N_i(x) dx \right]}. \quad (1.8)$$

26 The sum is over all species i with frequency-dependent absorption or scattering cross-
 27 section $\sigma_i(\nu)$ and line-integrated number density $\int_0^d N_i(x) dx$. When considering a narrow
 28 frequency interval, the frequency dependence of the scattering cross-sections and the mirror
 29 reflectivity can be neglected. In this case an effective loss factor R_{eff} is defined that includes
 30 not only the mirror losses, but also all broadband absorption and scattering losses.

31 In a CRDS experiment, the ring-down time, τ , is measured as a function of laser
 32 frequency ν . There are various ways in which the cavity decay rate can be extracted from
 33 the observed signal (these will be discussed in more detail below), but very often τ is
 34 obtained from a weighted least-squares fit to the light intensity decay transient. An
 35 absorption spectrum is obtained by plotting the cavity decay rate $k = 1/\tau$ or the cavity
 36 losses $1/c\tau$ as a function of frequency:

$$38 \quad \frac{1}{c\tau(\nu)} = \frac{1-R}{L} + \alpha(\nu) \frac{d}{L} \quad (1.9)$$

40 This cavity loss is the sum of two terms, one is the mirror loss and determines the base line of
 41 the CRD spectrum, i.e. $(1-R)/L$, and the other term includes the absorption, i.e. $\alpha d/L$.
 42 Therefore, the absorption due to the sample in the cavity is obtained by subtracting the
 43 off-resonance loss ($k_0 = 1/\tau_0 = c(1-R)/L$) from the on-resonance loss:

$$45 \quad \alpha(\nu) \frac{d}{L} = \frac{k-k_0}{c} = \frac{1}{c\tau} - \frac{1}{c\tau_0} = \frac{\tau_0 - \tau}{c\tau_0\tau} \quad (1.10)$$

1 This relationship shows that the absorption is determined by the measurement of two decay
 2 rates or ring-down times. For gas phase samples, the width of an absorption feature is
 3 typically much narrower than the spectral range ($\sim 1\%$ fractional change in wavelength)
 4 over which the mirror reflectivity changes significantly. In that case, the mirror loss can be
 5 treated as a constant baseline, fitted as in traditional absorption spectroscopy (see Chapter
 6 3). Alternatively, when dealing with intrinsically very broad absorptions, the cavity decay
 7 rate can be measured with and without sample and the difference is used to determine $\alpha(\nu)$.
 8 It is interesting to note that if the sample fills the cavity ($d=L$), the sample absorption
 9 coefficient $\alpha(\nu)$ can be calculated without knowledge of the sample length. In that case,
 10 one only needs to measure two ring-down times in order to determine the absolute value
 11 of the absorption coefficient!

12 The minimum detectable absorption in CRDS can be written as:

$$13 \quad \left[\alpha(\nu) \frac{d}{L} \right]_{\min} = \frac{\Delta k_{\min}}{c} = \frac{1}{c\tau_0^2} \Delta\tau_{\min} = \frac{1-R}{L} \left(\frac{\Delta\tau}{\tau_0} \right)_{\min} \quad (1.11)$$

16
 17 The smallest absorption coefficient that can be measured is proportional to the smallest
 18 fractional change in k that can be detected, which in turn is proportional to the mirror loss
 19 divided by the cell length if a constant fractional change in τ can be detected. Thus, it would
 20 appear that higher reflectivity mirrors and longer spacing would increase sensitivity. This is
 21 true up to a point, but one must also consider that the fraction of light that gets through the
 22 cell will also decrease with only small increase in ring-down time once the sample loss
 23 (including, for example, scattering losses) exceeds the mirror loss. At atmospheric pressure,
 24 Rayleigh scattering by a gaseous sample can be a significant loss. In fact, R in this equation
 25 is actually the aforementioned R_{eff} , which is less than (or equal to) the reflectivity of the
 26 mirrors.

27 The sensitivity can also be increased by increasing the accuracy of the determination of
 28 the ring-down time, thus minimizing $\Delta\tau/\tau$. Obviously, this is achieved by using a digitizer
 29 with the highest vertical (intensity) and horizontal (time) resolution to record accurately the
 30 ring-down transient, and a very good fitting routine to extract the ring down time or decay
 31 rate. However, in reality, the accuracy is often limited by the fluctuations in the shape of the
 32 ring-down transient, as will be discussed in the next section.

33 Equation (1.11) shows the essence of the sensitivity of CRDS. In order to achieve a high
 34 sensitivity in the absorption measurement, only a rather low accuracy in the time
 35 measurement is needed. For example, accuracy in the determination of τ of only 1%
 36 combined with a 10-cm-long cavity consisting of mirrors with a reflectivity of 99.99%
 37 leads to a minimum detectable absorption of 10^{-7} cm^{-1} . The effective path length in this
 38 example is one kilometer, and the ring-down time of the empty cavity is 3.3 μs .

39 Another important point is that CRDS is ideally independent of intensity noise on the
 40 excitation laser, as this will influence the amplitude of the ring-down signal but not its decay
 41 rate. During the decay, the intensity of the same pulse is compared after each round trip.
 42 Of course, one must be careful that the detection system is linear to high accuracy for this
 43 independence to hold strictly. Also, the CRDS sensitivity is independent of absorption that
 44 occurs along the optical path outside the optical cavity as long as it is not so strong as to
 45 attenuate the signal level substantially. Trace moisture concentration at parts per trillion
 46 (ppt) sensitivity has been detected, despite transmission of the optical beam through air that

1 contained a moisture concentration many orders of magnitude higher [19]. The only
 2 fundamental limit to the accuracy of the deduced cavity decay rate (and thus absorption
 3 coefficient) is shot noise, which causes the signal on the detector to have a noise that is
 4 proportional to the square root of the number of detected photons. The baseline noise (1σ)
 5 in the extracted α value is $(1 - R)/L$ times the square root of the number of photons detected
 6 during the decay [20]. The $(1 - R)/L$ factor equals the inverse of the mean photon path
 7 length in the sample and is often of the order of 10^{-5} – 10^{-7} cm^{-1} . The fraction of incident
 8 photons on the cavity that leave the back mirror, integrated over the decay, would be $(1 - R)/2$
 9 for ideal mirrors, but is more typically a factor of 10–100 less than this. However, that still
 10 translates to 10^8 – 10^{10} photons per decay for typical experimental conditions as used in
 11 most of the early experiments. Thus, the shot noise limit for the determination of the
 12 fractional cavity decay rate would be expected to be 10^{-4} – 10^{-5} . This should be reduced
 13 further by the square root of the number of decays that are observed at each spectral element.
 14 Alas, experience is that the fluctuations are typically much higher than this and $(\Delta\tau/\tau)_{\text{min}}$
 15 values of 0.1–0.001 are more typical. To understand the reasons for this, we must consider the
 16 wave nature of light inside the cavity.

17

18

19 1.4 A More Refined Picture

20

21 The simple description above has been called the ‘photon bullet model’ of CRDS. It
 22 captures the essence of CRDS in most cases, but has made a number of simplifications. Most
 23 importantly, the bullet model ignores the interference of light in the cavity. In fact, a CRDS
 24 cell is an etalon with a very high finesse. This implies that the cell will admit, from the
 25 broad bandwidth of the input pulse, only very narrow (few kHz in width) resonant modes.
 26 These resonant modes are characterized by the number of longitudinal nodes (each with a
 27 frequency separation of $c/2L$) and by the number of transverse nodes. The modes without
 28 transverse mode excitation are called TEM_{00} modes and, for a stable optical cavity,
 29 typically have a Gaussian shape characterized by a beam waist ω , which gives the distance
 30 from the axis where the field decreases by $1/e$. Higher order transverse modes are labeled
 31 TEM_{nm} , and these have n radial nodes and m angular nodal planes. These extend further
 32 from the optic axis by a distance that is proportional to the square root of $(n + 1)$. Such
 33 modes are separated from the TEM_{00} modes by a frequency shift proportional to $n + m$,
 34 though a small astigmatism in the cavity will cause a splitting of the degeneracy of modes
 35 with fixed $n + m$. The properties of the eigenmodes of a two mirror, linear, cavity (most
 36 often used for CRDS experiments) are discussed in Chapter 2. The text by Siegman [21]
 37 provides a thorough treatment. With minor adjustment, the theory of empty optical cavities
 38 carries over to those filled with a weakly absorbing material, as long as optical saturation
 39 (i.e. sample bleaching) can be neglected [22].

40 Excitation by a laser will excite each mode of the cavity with an intensity proportional to
 41 the spectral density of the input at the resonance frequency of the mode, and also
 42 proportional to the spatial overlap of the eigenmode with the input beam [22]. Each
 43 excited mode of the cavity will decay with its own decay rate and the light from different
 44 modes will, in general, interfere. Excitation of higher transverse modes can be dramatically
 45 reduced but not completely eliminated by ‘mode matching’, which means to shape the input
 46 beam so that it closely matches the size and radius of curvature of the TEM_{00} modes of the

1 cavity. This requires either a zoom telescope or a simple telescope with an adjustable
2 distance from telescope to cavity (see Chapters 2 and 10). The excitation efficiency of
3 different transverse modes to error in alignment or mode matching has been given in the
4 literature [22], and can be used to design an optical system. The fractional efficiency of
5 excitation of the TEM₀₀ mode cannot be greater than the inverse of the M^2 parameter of the
6 laser beam used to excite the cavity. M^2 is used to characterize beam quality ($M^2 = 1$ is an
7 ideal Gaussian mode) and is often given in the specification sheet of lasers. Many pulsed
8 lasers, especially dye lasers, have poor beam quality (large M^2), in which case the use of a
9 spatial filter, or another method to improve beam quality, is advised.

10 For an ideal cavity, the different transverse modes are orthogonal and thus no transverse
11 mode beating would be expected as long as the entire beam is detected (no clipping) with a
12 spatially uniform detector. In practice, some residual mode beating remains, both because
13 real detectors have some spatial dependence of their quantum efficiency and also because
14 the resonant modes are not orthogonal if there is a spatial dependence to the mirror loss,
15 which always occurs to some degree due to small defects in even the best mirror surfaces.
16 The latter can be observed by looking at the mirror surface with a modestly powered
17 microscope. One way to understand the transverse mode beating is that if the input beam
18 does not exactly match a single mode, then the shape and position of the beam on the mirrors
19 and detector will vary pass to pass. Mode beating is most problematic when the beating
20 frequency is close to the cavity mode decay rate, and so the cavity length should be adjusted
21 to avoid low-order rational ratios between the longitudinal and transverse mode separations
22 (which are exactly the separations used in a Herriott multipass cell). Even without the
23 deleterious effects of beating, excitation of higher transverse modes leads to instabilities
24 in the effective cavity decay rate as different transverse modes have different decay times.
25 One could anticipate that diffraction would cause this, but most CRDS experiments use
26 mirrors large enough for diffraction losses to be usually negligible for the low order
27 transverse modes [21]. Rather, the different sampling of the defects on the mirror surface by
28 different transverse modes is likely the principle cause. Experiments show that scattering
29 from the mirrors surfaces can couple the TEM₀₀ mode to very high order, but nearly
30 degenerate, transverse modes and cause periodic increases in the decay rate (much like
31 absorption lines!) as the modes tune through exact resonance with thermal drift of the cavity
32 length [23]. This can be overcome by use of an intracavity aperture that provides negligible
33 loss for the TEM₀₀ mode but high loss for high order modes. When exciting cavities with
34 narrow bandwidth light, from continuous wave (CW) lasers instead of pulsed lasers, the
35 excitation of higher modes can be greatly reduced if they are not within the line width of the
36 laser. This is likely the main reason that CRDS experiments with continuous wave lasers
37 often have an order of magnitude or lower shot-to-shot fluctuations in the extracted cavity
38 decay rate compared with pulsed lasers (see Chapter 2).

39 Excitation of different longitudinal modes of the cavity will lead to beating at the free
40 spectral range and its harmonics, far above the cavity decay rate and thus easily filtered out.
41 This mode beating describes the pulse traveling inside the cavity. However, if modes having
42 significantly different $\alpha(\omega)$ values are excited, then the decay will be multi-exponential
43 with each mode decaying at its own rate. This so-called 'bandwidth effect' is present in
44 pulsed CRDS experiments where a narrow absorption is detected with a broad bandwidth
45 laser. Suppose the laser wavelength is set at the center of the absorption. Then, light with
46 a wavelength at the center will have a short decay time, whereas wavelengths in the wings

1 of the laser profile will have a decay time close to that of the empty cavity. If the decay
2 rates are very similar, then the fitted decay rate will be a weighted average of those of the
3 excited modes, but for substantial differences (say more than 10 %), the effective decay rate
4 is not even well defined since it will change depending on how the decay transient is fitted.
5 In general, an absorption is underestimated if the bandwidth of the laser is comparable to or
6 larger than the width of the absorption. Note that this 'bandwidth effect' is analogous to the
7 well-known effect in traditional absorption spectroscopy where Beer's law does not hold
8 when the instrument resolution is insufficient. This is best resolved by increasing the
9 resolution of the laser and/or using pressure broadening to increase the width of the
10 individual lines. Alternatively, if the laser line shape is well characterized, then one can
11 simulate the decay as a multiple exponential decay and fit it as the real data to correct for
12 these 'curve of growth' effects (for a review, see Reference [18]). In another approach one
13 limits the determination of the ring-down time to the first part of the decay transient where it
14 is still single exponential. This is equivalent to the small absorption limit discussed
15 before. Furthermore, Zalicki and Zare [24] have shown that for small absorptions the
16 measured integrated absorption deviates only slightly from the true integrated absorption,
17 again as in a traditional absorption measurement. Several authors have investigated the
18 bandwidth effect in CRDS [18,24–27].

19 In principle, since the cavity is in fact a highly selective filter, CRDS is sensitive to
20 sample absorption only at the excited modes, which are typically much narrower than the
21 width of even most single mode lasers. Hodges and coworkers exploited this effect
22 (by locking the cavity modes to a stabilized reference laser [28]) to improve dramatically
23 the accuracy of the determination of absorption cross-sections, pressure broadening of line
24 widths, and pressure-induced shifts of individual rovibronic transitions [29]. In the visible
25 and UV spectral region, the longitudinal mode spacing of the cavities used in CRDS
26 ($\sim 100\text{--}300$ MHz) is much narrower than even most Doppler broadened lines, and thus the
27 finite sampling of the line shape causes only minor errors. However, as one moves to the IR
28 and Doppler widths narrow, substantial distortion can occur unless one is dealing with
29 intrinsically broader features. Off-axis excitation of the CRDS cavity, with a cavity length
30 selected such that the ratio of longitudinal and transverse mode spacings is irrational,
31 allows the transmission spectrum of the cavity to be made much more dense [30], thus
32 minimizing this effect. The effective mode spacing is reduced by a factor of the number of
33 cavity round trips before the intracavity beam has substantial overlap with that of the first
34 pass. The 'price' of this configuration is that the many modes excited beat against one
35 another and also have different decay rates (due to mirror reflectivity variations and perhaps
36 also diffraction), which increases the baseline noise.

37 A sample with wavelength dependent loss also has dispersion. The Kramers–Kronig
38 relationship, relate the two effects. This dispersion leads to a very slight shift of the
39 resonance frequency of the cavity modes [31]. However, for the extremely small sample of
40 absorptions studied by CRDS, these shifts are tiny and largely negligible. It is interesting,
41 however, that these shifts are required to predict properly the time-dependent shape of a
42 short pulse propagating inside the cavity [31]. The dielectric mirrors themselves introduce
43 some cavity dispersion, which changes the cavity mode spacing. Linear dispersion
44 changes the spacing by a constant factor and is thus equivalent to a small change in cavity
45 length. Higher order dispersion creates a frequency dependence on the spacing. These shifts
46 are negligible for routine spectroscopic work, but they are very important if one wants

1 efficiently to couple a laser source with a spectral frequency comb with a CRDS cavity.
2 Such combs are generated by mode locked lasers. The recent development of self-
3 referenced, frequency-locked, combs allows a dramatic improvement in frequency metrol-
4 ogy. The Jun Ye group is exploiting these sources for CRDS measurements [32].

5 It is worthwhile at this point to mention some other effects that can introduce noise or
6 reduce the accuracy of CRDS measurement of sample absorption. One is that many pulsed
7 lasers contain a broad bandwidth Amplified Spontaneous Emission (ASE) component in
8 addition to the narrow-band emission. This ASE can contribute to the decay transient,
9 perhaps disproportionately since some of it could be in the wings of the mirror high
10 reflectivity spectral region and thus have higher injection efficiency into the cavity.
11 Such ASE is particularly problematic when using a Ti:sapphire or similar solid-state laser
12 with a long fluorescence lifetime, which can be comparable with the cavity decay time.
13 A Brillouin scattering cell used as a phase conjugate reflector dramatically reduces the ASE
14 and also improves the quality of the beam as well [20]. If this cannot be used, a grating or
15 narrow band interference filter can be used to suppress ASE reaching the cell. Without such
16 corrections, the spectra can look great but the accuracy of absolute intensities will suffer.

17 Another important effect is that any feedback of light leaving the cavity (from any mirror)
18 that is back reflected into the cavity mode will interfere with light inside the cavity. It is
19 perhaps counter intuitive that even a 0.1 % reflection back to a 99.99 % reflectivity mirror
20 could produce a few percent modulation in the cavity decay rate [20]. One should use
21 wedged optics for CRDS mirrors so that the back reflection from the mirror outside surface
22 is deflected enough (a few mrad is sufficient) for the overlap with the TEM₀₀ mode to be
23 negligible. If wedged mirrors are not available, aligning the cavity such that the optic axis
24 strikes away from the center of the mirror can make a curved mirror into an effectively
25 wedged optic [19], although one must be careful not to get too close to the edge since often
26 the super polish of the substrate covers only the central part of the mirror. Any lens or other
27 optical elements in the path should be tilted to prevent feedback to the cavity and the
28 detector adjusted off axis as well. A ring optical cavity has an advantage in this regard as any
29 back reflection is coupled in the oppositely traveling mode.

30 Scattering loss from small particles is a potential source of noise. A single 1 micrometer
31 particle in the beam can introduce a loss per pass of ~ 1 ppm, which is substantially larger
32 than the noise in the decay rate, which can be ~ 10 ppb [33]. If at all practical, one should use
33 fine particle filters in the gas flow into the CRDS cell in order to minimize such effects
34 (unless using CRDS to detect particle scattering!). Gas flow should be kept sufficiently low
35 as to prevent turbulence in the intracavity flow, as density variations cause unstable optical
36 loss and thus noise in the measurements. It is found that the loss of the mirrors is very
37 sensitive to thin films deposited from the gas on the surface. Rapid evacuation of the CRDS
38 cell should be avoided as this cools the gas, which can lead to deposits that do not come off
39 even after long pumping times, as demonstrated by increased cavity decay rates. The mirror
40 loss is often found to be strongly temperature dependent, likely also due to gas absorption on
41 the mirror surface and so temperature control of the CRDS cell is advised if one wishes to
42 compare decay rates widely separated in time, such as when studying broad absorption
43 features.

44 Lastly, in terms of optical effects, it is noted that even the best mirrors have residual
45 birefringence of a few μrad or less per bounce. Mounting the mirrors can easily introduce
46 additional strain birefringence. This means that the polarization state of the light will rotate

1 as it rings down and so one needs to avoid using any polarization selective elements after the
 2 cavity [34]. This is not possible if the goal is to measure the sample-induced change of the
 3 polarization of the intracavity light, either induced by an external magnetic field [35,36] or
 4 due to chirality of the sample [37]. Experiments have been reported that show that the decay
 5 rate (even without polarization analysis after the cell) can be dependent upon the
 6 polarization of the input [34]. Likely, this is due to polarization sensitive scattering loss
 7 from mirror defects. Furthermore, with free space propagation, the polarization state of the
 8 input beam is typically stable, but not if a nonpolarization-maintaining optical fiber is used.

9
 10

11 1.5 Fitting of Cavity Ring-Down Transients

12

13 A key part of any CRDS experiment is the method used to determine the decay rate of
 14 intracavity light from the time-dependent signal on the optical detector. The sensitivity of
 15 the experiment will be directly proportional to the fluctuations of the cavity decay rate
 16 extracted shot-to-shot (i.e. on different cavity decays that are observed). We also want an
 17 unbiased method, in that after averaging many decays, at fixed intracavity loss, the average
 18 extracted decay rate converges on the true value. A wide variety of both digital and analog
 19 signal processing methods has been used for CRDS, often with conflicting claims of
 20 superiority. This section is not a review of those methods. A short review on the analysis of
 21 ring-down decays is available [38]. Here, we summarize the findings of the study by
 22 Lehmann and Huang [39].

23 We should begin with an analysis of the intrinsic noise sources. These are detector noise,
 24 characterized by its Noise Equivalent Power, P_N (with units of watts per root Hz), and shot
 25 noise in the optical signal, which has a spectral density of the square root of $(h\nu P(t)/Q)$
 26 where ν is the optical frequency of the light, $P(t)$ the power on the detector at time t , and Q
 27 the quantum efficiency of the detector. While both contribute, the fitting of real data is
 28 greatly simplified if one assumes that one of these sources dominates. Fortunately, though
 29 we assume different weights to the data points depending upon the assumed noise source, in
 30 practice, making an incorrect assumption does not introduce bias (i.e. error) and only
 31 modestly increases noise.

32 The ‘gold standard’ (theoretically lowest possible noise) is to use an Analog to Digital
 33 (AD) converter or digital oscilloscope to digitize the detector decay signal with rate $1/\Delta t$ and
 34 then do a weighted least squares fit to the resulting signal. Press *et al.* [40] provide a good
 35 introduction the theory behind least-squares fitting. The AD should have a sufficient
 36 number of bits (resolution) such that the least significant bit (often called the digitization
 37 noise) is below the noise on the detector. Usually a 12-bit resolution is sufficient but 8 bits is
 38 not. The digitization rate should be selected such that $k\Delta t$ is $\ll 1$, that is, we have many
 39 points per cavity decay time, though there is minimum improvement when below 0.1
 40 (assuming correct filtering, as shown below). Any noise in the input at frequencies above the
 41 Nyquist limit ($1/2\Delta t$) will be aliased to lower frequencies by the digitization (a noise
 42 component a $1/\Delta t$ will appear as a DC signal). Thus, the analog signal entering the AD
 43 converter should be low pass filtered with a longest time constant of one or two times Δt ,
 44 which ensures that aliased frequencies contain little noise power. Such filtering will
 45 produce minimal distortion of the early part of the ring-down signal. The detector should
 46 not be AC coupled as this will distort the signal at long times.

1 The data is fit to a functional form $A \exp(-kt) + B$. If the DC level of the detector (B) is
 2 sufficiently stable, it is best to treat that as a fixed value in the fitting of the decays; in that
 3 case, there is little improvement when the signal is fitted beyond three (6) decay times when
 4 the noise is dominated by detector (shot) noise. When the DC level of the detector is not
 5 sufficiently stable, then the fit should include an adjustable baseline, but then at least 10 time
 6 constants should be fit to minimize correlation of the decay rate with the offset. It is also our
 7 experience that the very beginning of the decay is often distorted and starting the fit after a
 8 time delay can reduce fluctuations of the cavity decay rate. We have also experienced
 9 distortions of the detector, amplifier and/or AD converter at full value and have also found
 10 it useful to start the fit only when the signal has decayed to some fixed value.

11 The fit to an exponential form is a nonlinear fit in the decay rate parameter and thus
 12 in general is iterative. However, starting with a rough ($\sim 10\%$) estimate of the decay rate,
 13 two iterations are sufficient to obtain convergence to $\sim 0.01\%$, below the precision of most
 14 experiments. There have been several papers published proposing alternative numerical
 15 fitting methods that are claimed significantly to decrease the computational effort required
 16 to extract a cavity decay rate. These appear to offer substantial improvement if compared
 17 with a black box least squares fitting package. However, if one assumes one is either
 18 detector or shot noise dominated, an optimized least squares fit routine that exploits
 19 geometric series to calculate many of the required terms with summing is faster than the
 20 alternatives that have been proposed. Also, it often has significantly lower noise and bias.
 21 We recommend doing a least squares fit to the CRDS intensity decay data whenever
 22 practical. With software written in BASIC running on a Windows PC, 1000 decays per
 23 second (each with 2000 points) can easily be analyzed. LabView programs are notoriously
 24 slow and should be avoided.

25 When averaging multiple decays to extract a ring-down rate, there is the option of fitting
 26 each decay and averaging the decay rates, or averaging the decay signal and then fitting
 27 once. For ideal Gaussian noise, the two approaches are equivalent and the second is faster.
 28 However, experience shows that there are often some ‘bad decays’ that are outliers. Often
 29 these can be rejected simply on the basis of high chi-squared values of the fit; standard
 30 statistical methods of outlier rejection, such as Chauvenet’s criteria [41] can also be used.
 31 The standard deviation of the decay rates provides a reliable estimate of the standard error
 32 (uncertainty) of the mean decay rate. If the decay signals are averaged before fitting, it is
 33 much harder to detect bad decays and even if detected, good data has to be eliminated to
 34 remove the bad. It is advised to fit each decay and use goodness of fit and outlier tests to
 35 make the decay rate estimate robust to outliers. If more decays are observed than can be fit or
 36 transferred to the computer, some averaging before fitting should be done but it should
 37 still be minimized.

38 When the decay is shot noise limited, the predicted standard error in the extracted cavity
 39 decay rate is $\sigma(k) = \sqrt{k^3 \frac{h\nu}{Q \cdot I(0)}}$ where $I(0)$ is the signal (in watts) on the detector at the start
 40 of the ring-down transient (or the start of the fitting window) and Q is the quantum
 41 efficiency of the detector. In the case of pulsed excitation of the cavity, $I(0) = \frac{T^2}{t_r} J$ where T
 42 is the mirror transmission, t_r is the cavity round trip time, and J is the energy per pulse at the
 43 input to the cavity. Division of the decay rate noise by c gives the noise in the sample
 44 absorption. When using photoconductive detectors, particularly in the IR, the signal will
 45 often be detector noise limited. In this case, optimal fitting predicts $\sigma(k) = \sqrt{8k^3 \frac{P_N}{I(0)}}$ and
 46 thus the sensitivity scales inversely with the initial signal-to-noise ratio of the decay.

1 In practice, mode beating, feedback to the cavity, and other effects will often increase the
2 shot-to-shot fluctuations in the cavity decay rate. It is advised that the shot and detector
3 noise limits be estimated for any experiment, since that will give the experimenter an
4 estimate of how much the experimental sensitivity could be improved. The above
5 calculations are for the sensitivity per shot. Ideally, the standard deviation in k will
6 decrease as the square root of the number of decays rates that are averaged. In practice, this
7 holds for some time but after that drift starts to dominate the noise. This maximum effective
8 averaging time can be determined by collecting a large data set at one wavelength and then
9 computing an Allen Variance [42]. The interval corresponding to the minimum on such a
10 plot gives this time and the minimum itself gives the maximum sensitivity that can be
11 obtained by signal averaging.

12 There are several analog detection methods that have been described in the literature.
13 Noise propagation calculations reveal that these have higher noise than the least squares fit
14 method, though only modestly so for most. Their principle disadvantage is that they do not
15 allow for the robust outlier rejection that is described above. Their advantage is that they do
16 not require the processing of lots of data and therefore are useful when using very high
17 repetition rate lasers (say > 10 kHz), where fitting each individual decay becomes
18 impractical. Perhaps most widely used is the phase shift method. In this method, the input
19 light intensity is amplitude modulated, ideally by 100 %, at some fixed frequency Ω
20 (optimal is $\Omega \sim \tau^{-1}$). One measures the cavity transmission with a vector or dual channel
21 lock-in amplifier and determines the phase shift, ϕ , between the modulation of the light
22 input and that transmitted by the cavity. The cavity decay time, τ , can be calculated from
23 $\tan \phi = \Omega\tau$. This method was used, even before the explicit cavity decay, to measure the loss
24 of super mirrors, and was first used in CRDS measurements by Engeln *et al.* [43]. When the
25 cavity is excited by a series of pulses that are short compared with the decay time, the phase-
26 shift method is, like regular CRDS, insensitive to laser intensity noise. However, if a 50 %
27 duty cycle chopped laser is used, laser intensity noise does contribute. Phase-shift CRDS is
28 discussed in more detail in Chapter 2. The phase shift method is not appropriate when using
29 a pulsed laser with repetition rate far below the cavity decay rate. Romanini and
30 Lehmann [20] used the log of the ratio of the cavity transmission sampled by two gated
31 integrators. The Zare group has used a log amplifier to produce a voltage proportional to the
32 cavity decay rate [44].

33

34

35 1.6 A Few Examples

36

37 This section provides a few examples of pulsed CRDS experiments not mentioned in the
38 other chapters. They have been selected to illustrate the capabilities of CRDS. Figure 1.4
39 shows a CRD spectrum of laboratory air around 253.7 nm [25], which demonstrates the
40 capabilities of CRDS in terms of measuring weak absorptions of abundant species
41 (molecular oxygen) and using strong transitions to detect trace gas species (mercury).
42 The open cavity consisted of two mirrors with a reflectivity of 99.7 % and a radius of
43 curvature of 25 cm, spaced at distance of 45 cm. The laser was a frequency doubled pulsed
44 dye laser with a bandwidth of 0.1 cm^{-1} . The absolute absorption of mercury and oxygen is
45 easily obtained from this spectrum, since the vertical axis displays the cavity losses $1/c\tau$ (see
46 Equation (1.9) with $d=L$). From the known cross section of $3.3 \times 10^{-14} \text{ cm}^2$ for this

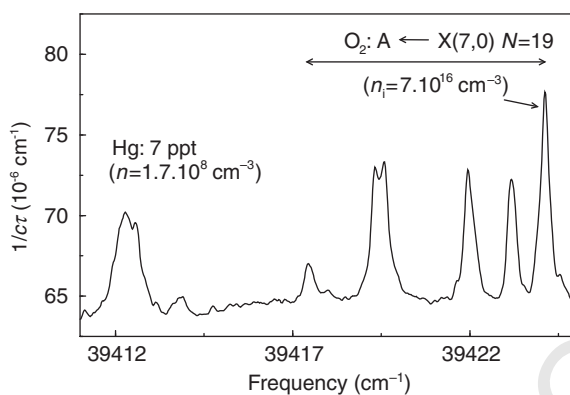


Figure 1.4 Cavity ring-down spectrum of laboratory air recorded around 253.7 nm. It demonstrated the capabilities of CRD spectroscopy: the measurement of trace gas species (mercury) by probing strong transitions, and the measurement of very weak transitions of abundant species (molecular oxygen). Reprinted with permission from [25]. Copyright 1995, American Institute of Physics

mercury line, the natural background concentration of mercury in the laboratory was determined to be 7 ppt.

Figure 1.5 shows the CRD spectrum of the $106 \leftarrow 000$ transition of HCN where one quantum in the CN stretch, none in the bending mode, and six quanta in the CH stretch were excited using laser light around 492 nm. By recording this very weak overtone band at different pressures, it was shown by Romanini and Lehmann [20] that there is a large collisional line-mixing effect in the proximity of the R branch heads.

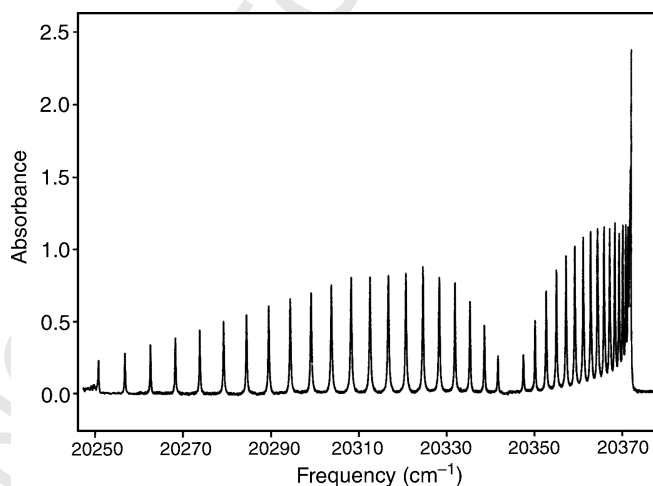


Figure 1.5 The cavity ring-down absorption spectrum of the $106 \leftarrow 000$ transition of HCN measured at a sample pressure of 100 torr. Reprinted with permission from [20]. Copyright 1993, American Institute of Physics

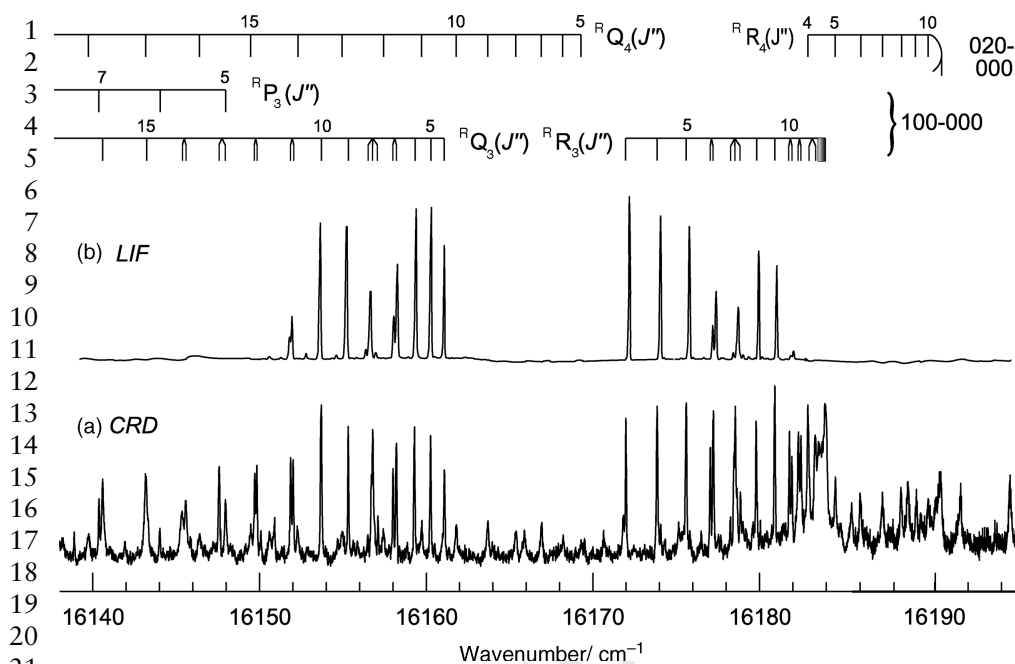


Figure 1.6 The cavity ring down absorption spectrum (a) and laser induced fluorescence spectrum (b) of the HNO molecule. Transitions are from the ground state to the vibrational levels (100) and (020) of the \tilde{A}^1A'' excited state. The spectra are not identical because predissociation of certain levels in the excited state prevents fluorescence. Reprinted with permission from [47]. Copyright 1997, American Institute of Physics

The combination of CRDS with laser-induced fluorescence (LIF) has been applied by several groups for different applications. For example, Dreyer *et al.* [45] used the CRD spectrum of the $-OH$ radical to calibrate the simultaneously recorded LIF spectrum of $-OH$ in a premixed atmospheric pressure flame. Using this combined approach, the Meijer group determined predissociation rates of the $-OH$ radical [46] and Pearson *et al.* studied the predissociation dynamics of HNO [47]. Spectra presented in the latter study are shown in Figure 1.6. Much of the structure present in the CRD spectrum is absent in the LIF spectrum because of predissociation of the electronically excited state.

The use of CRDS in studying reaction kinetics was first explored by Yu and Lin [48], who investigated the kinetics of the $C_6H_5 + O_2$ reaction. For slow reactions, where the concentration of the detected species can be regarded as constant during the ring-down transient, the ring-down transient is a single exponentially decaying function. In this case, the CRD absorption measurement is performed as described before. The concentration is obtained from the ring-down time, and a concentration–time profile (needed to determine the rate constant) is obtained by absorption measurements as a function of time after the reaction is initiated with, for example, a photolysis laser. For fast reactions, the ring-down transient becomes nonexponential owing to a changing concentration during the ring-down event. In that case, special models are needed to fit the non-exponential ring-down event

1 in order to extract the rate constants for the reaction [49]. CRDS for quantitative gas-phase
2 kinetic measurements has been reviewed by Friedrichs [18].

3 Although most CRDS experiments are performed with linearly polarized light, the
4 polarization state is not explicitly used. By placing polarization selective optical compo-
5 nents before and behind the ring-down cavity, the linear or circular dichroism in molecular
6 systems can be measured.

7 The rotationally resolved spectra of the A band of molecular oxygen have been recorded
8 in magnetic fields up to 20 tesla, in order to validate the theoretic model that is used
9 to describe the interaction between oxygen molecules and the magnetic field [36].
10 Experiments have been performed with a 3-cm ring-down cavity, which is placed in the
11 homogeneous part of the magnetic field. Comparison of the spectra recorded with linearly,
12 right-hand circularly, and left-hand circularly polarized light show that the polarization
13 state of the light is not (or hardly) affected by the multiple reflections on the cavity mirrors.

14 By placing a polarization selective optical element in front of the detector (for example a
15 polarizer), it is possible to measure the rotation of the plane of polarization of the incoming
16 linearly polarized beam upon passage through the ring-down cavity. Magneto-optical
17 effects can be measured by placing the cavity inside a magnetic field; the plane of
18 polarization can rotate owing to dispersion (magnetic birefringence) or polarization
19 dependent absorption (magnetic dichroism). As in CRDS, where the rate of absorption
20 is measured, in the polarization-dependent scheme the rate of optical rotation is measured.
21 Optical rotation can thus be measured on an absolute scale. Polarization dependent cavity
22 ring down spectroscopy (PD-CRDS) has been used to study magneto-optical effects in
23 molecular oxygen [35,36] and the polarization rotation as a result of the Faraday effect in a
24 BK7 window [35]. In a magnetic field of 2 mT, the polarization rotation in a 2-mm-thick
25 BK7 window placed inside the ring down cavity was 2×10^{-5} rad/passage.

26 Without an external magnetic field, the overall polarization rotation will cancel out
27 during each round trip through the cavity. In order to measure field free polarization
28 rotation, the direction of the optical rotation must be reversed upon each reflection at the
29 cavity mirror. This can be accomplished with two quarter-wave plates. Vaccaro and
30 coworkers [37] used this approach to measure the optical rotation and the differential
31 absorption induced by chiral compounds in the gas phase. They demonstrated a sensitivity
32 of 4×10^{-8} rad cm^{-1} , which is substantially better than the sensitivities for many
33 commercial polarimeters employed in solution phase studies.

34

35

36 1.7 Going Beyond the Standard Pulsed CRDS Experiment

37

38 In this introductory chapter, the simplest version of a CRDS experiment has been discussed.
39 It is easy to set up and has been used in undergraduate teaching laboratories. There are many
40 elaborations of this theme, which are discussed in the following chapters. Four of the most
41 commonly used experimental schemes are depicted in Figure 1.7. We here briefly discuss
42 some of the experimental considerations when applying these schemes.

43 In CRDS, the best sensitivity is obtained when a single longitudinal mode of the ring
44 down cavity is excited (see Section 1.3). Although not impossible, this single mode
45 excitation is difficult to achieve with pulsed lasers since they have a relatively large
46 bandwidth. The bandwidth of continuous wave (CW) lasers is typically below 10 MHz, and

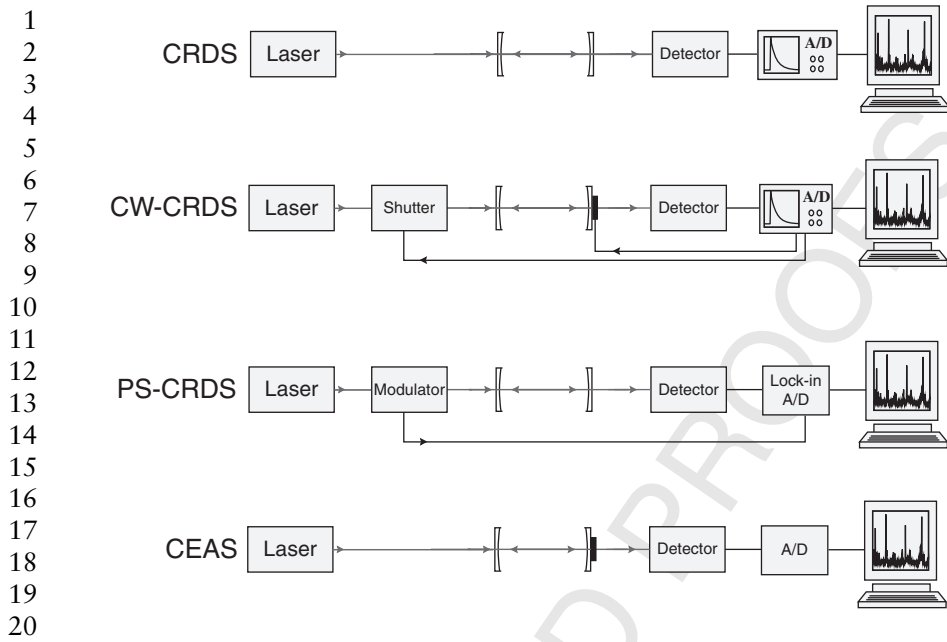


Figure 1.7 Sketches of four of the most commonly used CRDS schemes: pulsed CRDS, continuous wave CRDS (CW-CRDS), phase-shift CRDS (PS-CRDS), and cavity enhanced absorption spectroscopy (CEAS)

single longitudinal mode excitation can be achieved. In order to obtain a ring-down event, the laser frequency or cavity length must be tuned into resonance [50]. When the light on the detector exceeds some threshold value, a trigger signal is generated and the excitation of the cavity has to be terminated for ~ 5 – 10 cavity decay times. This can be done by turning off the laser drive current (in the case of diode lasers), or by using an intensity modulator such as an acousto-optical modulator (AOM) or a semiconducting optical amplifier (SOA) [42]. Recently, it has been demonstrated that the laser must be turned off with at least 70 db (i.e. to $<10^{-7}$ of its previous value) in order not to increase the noise [51]. Pockels cells and Mach-Zener modulators do not provide sufficient attenuation. The turn-off time constant for the light must be short compared with the cavity decay time, which eliminates (at least at present) MEMS type modulators. In the literature, CRDS performed with CW lasers is entitled CW-CRDS, but it should be realized that this technique is not a true CW technique at all. CW-CRDS is discussed in detail in Chapter 2. Compared with pulsed CRDS, CW-CRDS offers higher repetition rates (kHz), higher sensitivities (10^{-10} – 10^{-12} $\text{cm}^{-1} \text{Hz}^{-1/2}$) and, in most cases, higher spectral resolution. Furthermore, higher intracavity energies are achievable, resulting in higher intensities on the detector, thus improving the signal-to-noise ratios on the ring down transients. Additionally, the CW-CRDS schemes allow the use of compact, robust, and inexpensive diode lasers. Although a CW-CRDS experiment is (slightly) more complicated than a pulsed CRDS experiment, the aforementioned advantages are important enough so that for many applications, such as trace gas detection, CW-CRDS is the better choice. In this context, it is worth noting that all commercial cavity ring-down spectrometers employ one of the various CW-CRDS schemes.

1 A researcher who considers using CRDS should also consider the Cavity Enhanced
2 Absorption Spectroscopy (CEAS) method [52–54]. Here, one uses essentially the same
3 cavity as for CRDS. However, here we do not modulate the laser intensity but instead
4 measure the time-averaged transmission of the cavity. For the on-resonance excitation
5 of a cavity mode with a perfectly monochromatic light, the cavity transmission is inversely
6 proportional to the square of the cavity loss. However, the width of the mode also increases
7 as the loss, so if one excites using a radiation source with a line width much greater than the
8 cavity mode width (which is the case unless extremely narrow lasers are used), the average
9 transmission of the cavity scales inversely with the cavity loss. CEAS is clearly simpler
10 than CRDS to set-up and is particularly advantageous for use of continuous wave laser
11 sources, as then no intensity modulator is needed. This method, however, typically has
12 substantially higher noise. This is due both to the fact that one loses the intensity noise
13 immunity of CRDS and also because the excitation of each cavity mode is typically
14 stochastic. By exciting many transverse modes, the integrated noise is reduced. CEAS is
15 described in more detail in Chapter 2.

16 Another approach to cavity-enhanced spectroscopy is to combine the high sensitivity of
17 low loss cavities to additional loss with frequency modulation spectroscopy, a method
18 known as NICE-OHMS (see also Chapter 2). Here, one locks a very frequency-narrow laser
19 (<1 KHz) to one of the cavity resonances. This is a challenging task and usually requires use
20 of the Pound–Drever–Hall method. Then, one uses an electro-optic crystal on the input
21 beam to put sidebands on the laser at precisely the FSR of the cavity. Then all three waves
22 suffer the same phase shift upon transmission of the cavity and there is no intensity beating
23 at the cavity FSR. This is due to precise cancellation of the beats produced by the central
24 frequency (the carrier) with the upper and lower frequency sidebands. However, as in FM
25 spectroscopy described above, if either the upper or lower sideband has a differential
26 absorption or phase shift, the exact interference is lost and one gets a beating, the phase of
27 which tells which sideband had higher absorption. Because the transmission of each
28 frequency through the cavity is on the order of unity, instead of $1 - R$ as in pulsed CRDS,
29 this NICE-OHMS method has several orders of magnitude lower shot-noise. This is
30 primarily due to the much narrower lasers used in this method; CW-CRDS with the same
31 highly monochromatic laser would only have a factor of 2–3 lower shot noise. In addition,
32 the detection is at a high frequency that is above most the excess noise, including drifts in
33 cavity loss. In the JILA lab of Hall where this method was developed, the reported
34 sensitivity ($1 \times 10^{-14} \text{ cm}^{-1}$) was shot-noise limited and substantially higher than for any
35 CRDS experiment [55,56]. However, most following reports by other laboratories have
36 reported substantially lower sensitivity, similar in fact to the highest reported CRDS results
37 ($\sim 10^{-11} \text{ cm}^{-1}$). Also, because it determines the loss difference of two frequencies that
38 differ by two cavity FSRs, NICE-OHMS excels at detection of very narrow spectral
39 features, such as Lamb dips, but is not useful for spectra with broad spectral lines.

40 CRDS started with the development of ultra low-loss dielectric mirrors and the bulk of
41 work has continued to use cavities made from such optics. The mirrors themselves can be
42 immersed in most liquids for performing CRDS on species in solutions [57]. The mirrors are
43 fairly chemically inert (the top layer is often fused silica), but Lehmann’s group has
44 destroyed mirrors by putting them in strong acid solutions. The attainable path length in
45 liquids is typically limited, by bulk absorption and Rayleigh scattering, to lengths less than
46 1 km, but that can still be a big improvement over a standard 1-cm cuvette! An intracavity

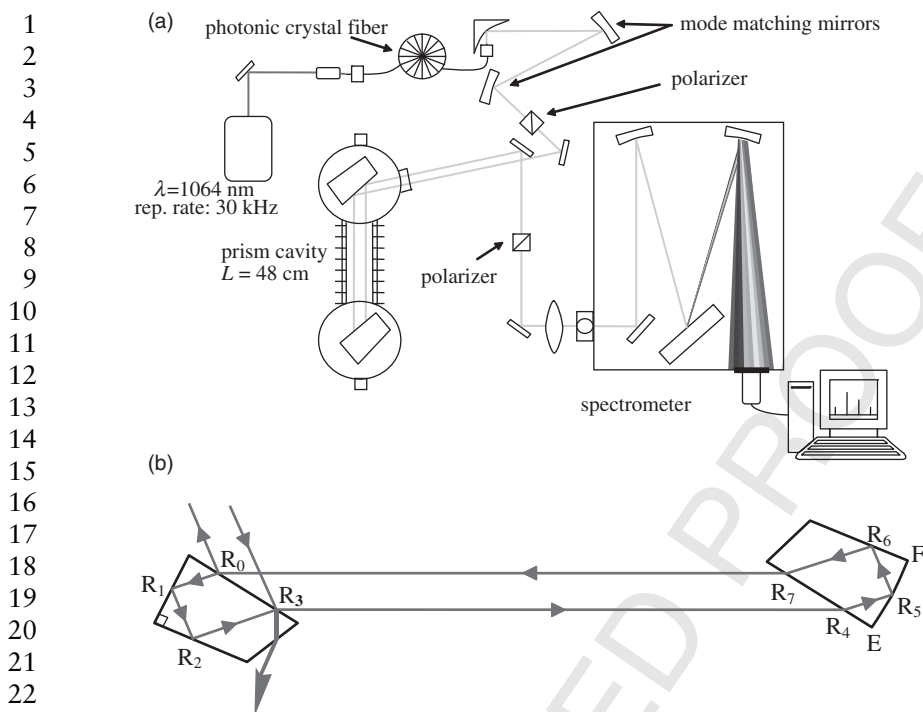
1 absorption cell can be used with the surfaces angled at the Brewster's angle [58], but it is
2 important to remember that the glass-liquid interface needs a different angle than the
3 glass-air one. Zare's group has used such a cell as a detector for liquid chromatography [59].
4 In the near-IR, the low loss of telecommunication fibers has been exploited by several
5 groups for CRDS measurements. Loock's group has used a fiber resonator with a small gap
6 to obtain CRDS of small liquid volumes [60]. Single-cell sensitivity arising from
7 optical scattering of the evanescent field surrounding the fiber has been demonstrated [61],
8 which opens the possible application of CRDS to biological sensing [62]. Cavity ring-down
9 spectroscopy with fibers is the subject of Chapter 5, while the application of CRDS to liquid
10 samples is discussed in Chapter 4.

11 A major recent center of CRDS activity has been the development of instruments that
12 cover a much wider spectral range than previously available. Incoherent light sources,
13 such as arc discharges and superluminal diodes, have been used as excitation sources
14 (see Chapter 3). The Lehmann group has been using the supercontinuum generated by
15 photonic crystal fibers (450–1700 nm in our case) when pumped by a small, high repetition
16 rate Nd:YAG laser. This source has very high spatial coherence and several orders of
17 magnitude higher spectral power density than other broad bandwidth sources. Jun Ye's
18 group [32] has worked closely with a mirror manufacturer to produce very low dispersion
19 mirrors that allow them simultaneously to inject light over a broad part of a stabilized
20 frequency comb.

21 To exploit the wide spectral range available with some of the new optical sources being
22 used for CRDS, one must move beyond the limitation of the standard narrow bandwidth
23 supermirrors. It is possible to use a stack of coatings with variable thickness to increase the
24 reflective bandwidth of mirrors. Newport Corp. is selling what they call broad bandwidth
25 supermirrors, which they specify with $R > 99.9\%$ over either the 485–700 or 700–910 nm
26 spectra ranges. Unfortunately, they only currently supply planar optics and thus they cannot
27 be used to build a CRDS cell but this shows what current mirror technology is capable of.
28 Certainly the increased number of layers increases absorption and scattering loss in such
29 mirrors. Also, the poor thermal conductivity of such thick stacks reduces the damage
30 threshold, which is important in pulsed CRDS experiments.

31 A different approach is to use prisms or other such structures. Pipino first used closed
32 resonances in a fused silica prism [63]. The intracavity light was deflected by total internal
33 reflection and coupled into and out of the cavity using frustrated total internal reflection.
34 He exploited such cavities for a number of studies of surface-bound species with sub-
35 monolayer coverage (see also Chapter 9). Recently, tremendous progress has been made
36 in the development of very low loss Whispering Gallery Mode Resonators [64]. In these,
37 light travels around the parameter of a toroidal cylinder. These hold great promise for
38 chemical sensing applications, particularly if the surface can be modified to provide highly
39 specific binding without compromising the low loss.

40 The Lehmann group has used fused silica Brewster-angle prism retroreflectors to build
41 broad bandwidth cavities. Intracavity light enters each prism at or very close to the Brewster
42 angle, undergoes two total internal reflections, and then leaves parallel to its direction
43 of entry (see Figure 1.8). A pair of such prisms (with one face figured with a 6-m radius of
44 curvature to provide focusing and thus give a stable optical cavity) forms a ring optical
45 cavity [65]. While the Brewster angle is wavelength dependent, the loss is quadratic for
46 small deviations from the Brewster angle. The fused silica prisms give a loss in the near-IR



24 **Figure 1.8** (A) Schematic of a cavity enhanced absorption spectrometer with a broadband
 25 Brewster angle retroreflector prism cavity. Broadband light is generated in a photonic crystal
 26 fiber. A grating spectrometer is used to disperse the light. (B) A schematic of the prism ring cavity
 27 showing the optical beam path. All surfaces are flat except EF which has a 6-meter convex
 28 curvature. Figure reproduced from Reference [65] with permission. Copyright 2008 Optical
 29 Society of America

31 within a factor of 10 of the highest reflectivity dielectric mirrors and cover a vastly larger
 32 bandwidth. As one moves into the visible, bulk Rayleigh scattering starts to dominate and
 33 leads to a λ^{-4} wavelength dependence. In principle, prisms fabricated from CaF_2 should
 34 have a more than an order of magnitude lower scattering loss in the visible and UV, while
 35 BaF_2 should allow extension into the mid-IR spectral region.

38 1.8 Summary

40 Cavity ring-down spectroscopy is a direct absorption technique; it provides the absorption
 41 coefficient on an absolute scale. There is no intrinsic limitation to the spectral region in
 42 which CRDS can be applied, as long as mirrors with a sufficiently high reflectivity,
 43 detectors with a sufficiently fast time response, and tunable light sources are available.
 44 CRDS has been applied at wavelengths between 197 nm [66] and 3.2 mm [67]. A sensitivity
 45 of 10^{-6} cm^{-1} can easily be obtained with a simple set-up. With some more effort, better
 46 sensitivities are reachable. With multi-mode excitation of the ring-down cavity, as in CRDS

1 with pulsed lasers and in CEAS with CW lasers, the sensitivity is in the range of
2 10^{-6} – 10^{-9} cm^{-1} . Single-mode excitation, as in CW-CRDS, offers the highest sensitivity:
3 10^{-7} – 10^{-12} cm^{-1} , and special variants can reach a sensitivity of 10^{-14} cm^{-1} [55]. These
4 sensitivities allow the detection of species in a variety of environments with CRDS, as will
5 be discussed in the following chapters.

6

7

8 **References**

9

- 10 [1] Anderson, D. Z.; Frisch, J. C.; Masser, C. S. Mirror reflectometer based on optical cavity decay
11 time, *Appl. Opt.* 1984, **23**, 1238–1245.
- 12 [2] Rempe, G.; Thompson, R. J.; Kimble, H. J.; Lalezari, R. Measurement of ultralow losses in an
13 optical interferometer, *Opt. Lett.* 1992, **17**, 363–365.
- 14 [3] Bilger, H. R.; Wells, P. V.; Stedman, G. E. Origins of fundamental limits for reflection losses
15 at multilayer dielectric mirrors, *Appl. Opt.* 1994, **33**, 7390–7396.
- 16 [4] Fowles, G. R. *Introduction to Modern Optics*, 2nd edition; Dover: 1975, see Chapter 4,
17 section 4.
- 18 [5] O’Keefe, A.; Deacon, D. A. G. Cavity ring-down optical spectrometer for absorption measure-
19 ments using pulsed laser sources, *Rev. Sci. Instrum.* 1988, **59**, 2544–2551.
- 20 [6] Scherer, J. J.; Paul, J. B.; O’Keefe, A.; Saykally, R. J. Cavity ringdown laser absorption
21 spectroscopy: history, development, and application to pulsed molecular beams, *Chem. Rev.*
22 1997, **97**, 25–51.
- 23 [7] Paldus, B. A.; Kachanov, A. A. An historical overview of cavity-enhanced methods, *Can. J.*
24 *Phys.* 2005, **83**, 975–999.
- 25 [8] Kritchman, E.; Shtrikman, S.; Slatkine, M. Resonant optoacoustic cells for trace gas analysis,
26 *J. Opt. Soc. Am.* 1978, **68**, 1257–1271.
- 27 [9] Lehmann, K. K.; Scherer, G. J.; Klemperer, W. Classical chaos and quantum simplicity: highly
28 excited vibrational states of HCN, *J. Chem. Phys.* 1982, **77**, 2853–2861.
- 29 [10] Harren, F. J. M.; Bijnen, F. G. C.; Reuss, J.; Voeselek, L. A. C. J.; Blom, C. W. P. M. Sensitive
30 intracavity photoacoustic measurements with a CO₂ wave-guide laser, *Appl. Phys. B.* 1990, **50**,
31 137–144.
- 32 [11] Kosterev, A. A.; Tittel, F. K.; Serebryakov, D. V.; Malinovsky, A. L.; Morozov, I. V. Applications
33 of quartz tuning forks in spectroscopic gas sensing, *Rev. Sci. Instrum.* 2005, **76**, 043105.
- 34 [12] Long, M. E.; Swofford, R. L.; Albrecht, A. C. Thermal lens technique: a new method of
35 absorption spectroscopy, *Science* 1976, **191**, 183–185.
- 36 [13] White, J. U. Long optical paths of large aperture, *J. Opt. Soc. Am.* 1942, **32**, 285–288.
- 37 [14] Herriott, D.; Kogelnik, H.; Kompfner, R. Off-axis paths in spherical mirror interferometers,
38 *Appl. Opt.* 1964, **3**, 523–526.
- 39 [15] Herriott, D.; Schulte, H. J. Folded optical delay lines, *Appl. Opt.* 1965, **4**, 883–889.
- 40 [16] Silver, J. A. Frequency-modulation spectroscopy for trace species detection: theory and
41 comparison among experimental methods, *Appl. Opt.* 1992, **31**, 707–717.
- 42 [17] Friedrichs, G. Sensitive absorption methods for quantitative gas phase kinetic measurements.
43 Part 1: Frequency modulation spectroscopy, *Z. Phys. Chem.* 2008, **222**, 1–30.
- 44 [18] Friedrichs, G. Sensitive absorption methods for quantitative gas phase kinetic measurements.
45 Part 2: Cavity ringdown spectroscopy, *Z. Phys. Chem.* 2008, **222**, 31–61.
- 46 [19] Dudek, J. B.; Tarsa, P. B.; Velasquez, A.; Wladyslawski, M.; Rabinowitz, P.; Lehmann, K. K.
Trace gas detection using continuous-wave cavity ring-down spectroscopy, *Anal. Chem.* 2003,
75, 4599–4605.
- [20] Romanini, D.; Lehmann, K. K. Ring-down cavity absorption spectroscopy of the very weak
HCN overtone bands with six, seven, and eight stretching quanta, *J. Chem. Phys.* 1993, **99**, 6287.
- [21] Siegman, A. E. *Lasers*, University Science Books; Mill Valley, CA, 1986.
- [22] Lehmann, K. K.; Romanini, D. The superposition principle and cavity ring-down spectroscopy,
J. Chem. Phys. 1996, **105**, 10263–10277.

- 1 [23] Huang, H. F.; Lehmann, K. K. Noise in cavity ring-down spectroscopy caused by transverse
2 mode coupling, *Opt. Express* 2007, **15**, 8745–8759.
- 3 [24] Zalicki, P.; Zare, R. N. Cavity ring-down spectroscopy for quantitative absorption measure-
4 ments, *J. Chem. Phys.* 1995, **102**, 2708–2717.
- 5 [25] Jongma, R. T.; Boogaarts, M. G. H.; Holleman, I.; Meijer, G. Trace gas detection with cavity
6 ring-down spectroscopy, *Rev. Sci. Instrum.* 1995, **66**, 2821–2828.
- 7 [26] Hodges, J. T.; Looney, J. P.; Van Zee, R. D. Laser bandwidth effects in quantitative cavity ring-
8 down spectroscopy, *Appl. Opt.* 1996, **35**, 4112–4116.
- 9 [27] Yalin, A. P.; Zare, R. N. Effect of laser lineshape on the quantitative analysis of cavity ring-down
10 signals, *Laser Physics* 2002, **12**, 1065–1072.
- 11 [28] Hodges, J. T.; Layer, H. P.; Miller, W. W.; Scace, G. E. Frequency-stabilized single-mode cavity
12 ring-down apparatus for high-resolution absorption spectroscopy, *Rev. Sci. Instrum.* 2004, **75**,
13 849–863.
- 14 [29] Robichaud, D. J.; Hodges, J. T.; Lisak, D.; Miller, C. E.; Okumura, M. High-precision pressure
15 shifting measurement technique using frequency-stabilized cavity ring-down spectroscopy,
16 *J. Quant. Spectrosc. Radiat. Transfer.* 2008, **109**, 435–444.
- 17 [30] Meijer, G.; Boogaarts, M. G. H.; Jongma, R. T.; Parker, D. H.; Wodtke, A. M. Coherent cavity
18 ring down spectroscopy, *Chem. Phys. Lett.* 1994, **217**, 112–116.
- 19 [31] Lehmann, K. K. Dispersion and cavity ring-down spectroscopy; In *Cavity-Ring-down Spectros-
20 copy*; Bush, K. W.; Bush, M. A.; editors; American Chemical Society: Washington, DC, 1999,
21 pp. 106–124.
- 22 [32] Thorpe, M. J.; Moll, K. D.; Jones, R. J.; Safdi, B.; Ye, J. Broadband cavity ring-down spectroscopy
23 for sensitive and rapid molecular detection, *Science* 2006, **311**, 1595–1599.
- 24 [33] Butler, T. J. A.; Miller, J. L.; Orr-Ewing, A. J. Cavity ring-down spectroscopy measurements of
25 single aerosol particle extinction. I. The effect of position of a particle within the laser beam on
26 extinction, *J. Chem. Phys.* 2007, **126**, 174302.
- 27 [34] Huang, H. F.; Lehmann, K. K. Effects of birefringence and polarization dependent loss of
28 supermirrors in cavity ring-down spectroscopy, *Appl. Opt.* 2008, **47**, 3817–3827.
- 29 [35] Engeln, R.; Berden, G.; Van den Berg, E.; Meijer, G. Polarization dependent cavity ring down
30 spectroscopy, *J. Chem. Phys.* 1997, **107**, 4458–4467.
- 31 [36] Berden, G.; Engeln, R.; Christianen, P. C. M.; Maan, J. C.; Meijer, G. Cavity ring down
32 spectroscopy on the oxygen a band in magnetic fields up to 20 tesla, *Phys. Rev. A* 1998, **58**,
33 3114–3123.
- 34 [37] Müller, T.; Wiberg, K. B.; Vaccaro, P. H. Cavity ring-down polarimetry (CRDP): a new scheme
35 for probing circular birefringence and circular dichroism in the gas phase, *J. Phys. Chem. A*
36 2000, **104**, 5959–5968.
- 37 [38] Mazurenka, M.; Orr-Ewing, A. J.; Peveall, R.; Ritchie, G. A. Cavity ring-down and cavity
38 enhanced spectroscopy using diode lasers, *Ann. Rep. Prog. Chem., Sect. C* 2005, **101**, 100–142.
- 39 [39] Lehmann, K. K.; Huang, H. F. Optimal signal processing in cavity ring-down spectroscopy;
40 In *Frontiers of Molecular Spectroscopy*; Laane, J., editor; Elsevier: Amsterdam, 2008.
- 41 [40] Press, W. H.; Teukolsky, S. A.; Vetterling, W. T.; Flannery, B. P. *Numerical Recipes*, Cambridge
42 University Press: Cambridge, 1986.
- 43 [41] Taylor, J. R. *An Introduction to Error Analysis*, Second edition, University Science Books:
44 Sausalito, 1982.
- 45 [42] Huang, H. F.; Lehmann, K. K. CW Cavity ring-down spectroscopy (CRDS) with a semicon-
46 ductor optical amplifier as intensity modulator, *Chem. Phys. Lett* 2008, **463**, 246–250.
- [43] Engeln, R.; Von Helden, G.; Berden, G.; Meijer, G. Phase shift cavity ring down absorption
spectroscopy, *Chem. Phys. Lett.* 1996, **262**, 105–109.
- [44] Spence, T. G.; Harb, C. C.; Paldus, B. A.; Zare, R. N.; Willke, B.; Byer, R. L. A laser-locked
cavity ring-down spectrometer employing an analog detection scheme, *Rev. Sci. Instrum.* 2000,
71, 347–353.
- [45] Dreyer, C. B.; Spuler, S. M.; Linne, M. Calibration of laser induced fluorescence of the OH
radical by cavity ringdown spectroscopy in premixed atmospheric pressure flames, *Combust.
Sci. Technol.* 2001, **171**, 163–190.

- 1 [46] Spanjaars, J. J. L.; Ter Meulen, J. J.; Meijer, G. Relative predissociation rates of OH ($A^2\Sigma^+$,
2 $v^1 = 3$) from combined cavity ring down–laser-induced fluorescence measurements, *J. Chem.*
3 *Phys.* 1997, **117**, 2242–2248.
- 4 [47] Pearson, J.; Orr-Ewing, A. J.; Ashfold, M. N. R.; Dixon, R. N. Spectroscopy and predissociation
5 dynamics of the \tilde{A}^1A' state of HNO, *J. Chem. Phys.* 1997, **106**, 5850–5873.
- 6 [48] Yu, T.; Lin, M. C. Kinetics of the $C_6H_5 + O_2$ reaction at low temperatures, *J. Am. Chem. Soc.*
7 1994, **116**, 9571–9576.
- 8 [49] Brown, S. S.; Ravishankara, A. R.; Stark, H. Simultaneous kinetics and ring-down: rate
9 coefficients from single cavity loss temporal profiles, *J. Phys. Chem. A* 2000, **104**, 7044–7052.
- 10 [50] Romanini, D.; Kachanov, A. A.; Sadeghi, N.; Stoeckel, F. CW cavity ring down spectroscopy,
11 *Chem. Phys. Lett.* 1997, **264**, 316–322.
- 12 [51] Huang, H.; Lehmann, K. K. Noise caused by a finite extinction ratio of the light modulator in CW
13 cavity ring-down spectroscopy, *Appl. Phys. B* 2009, **94**, 355–366.
- 14 [52] Engeln, R.; Berden, G.; Peeters, R.; Meijer, G. Cavity enhanced absorption and cavity enhanced
15 magnetic rotation spectroscopy, *Rev. Sci. Instrum.* 1998, **69**, 3763–3769.
- 16 [53] O’Keefe, A.; Scherer, J. J.; Paul, J. B. CW integrated cavity output spectroscopy, *Chem. Phys.*
17 *Lett.* 1999, **307**, 343–349.
- 18 [54] Peeters, R.; Berden, G.; Apituley, A.; Meijer, G. Open-path trace gas detection of ammonia based
19 on cavity-enhanced absorption spectroscopy, *Appl. Phys. B* 2000, **71**, 231–236.
- 20 [55] Ye, J.; Ma, L. -S.; Hall, J. L. Ultrasensitive detection in atomic and molecular physics:
21 demonstration overtone spectroscopy, *J. Opt. Soc. Am. B* 1998, **15**, 6–15.
- 22 [56] Ma, L. -S.; Ye, J.; Dubé, P.; Hall, J. L. Ultrasensitive frequency-modulation spectroscopy
23 enhanced by a high-finesse optical cavity: theory and application to overtone transitions of C_2H_2
24 and C_2HD , *J. Opt. Soc. Am. B* 1999, **16**, 2255–2268.
- 25 [57] Hallock, A. J.; Berman, E. S. F.; Zare, R. N. Direct monitoring of absorption in solution by cavity
26 ring-down spectroscopy, *Anal. Chem.* 2002, **74**, 1741–1743.
- 27 [58] Xu, S. C.; Sha, G. H.; Xie, J. C. Cavity ring-down spectroscopy in the liquid phase, *Rev. Sci.*
28 *Instrum.* 2002, **73**, 255–258.
- 29 [59] Snyder, K. L.; Zare, R. N. Cavity ring-down spectroscopy as a detector for liquid chromatography,
30 *Anal. Chem.* 2003, **75**, 3086–3091.
- 31 [60] Tong, Z. G.; Jakubinek, M.; Wright, A.; Gillies, A.; Loock, H. P. Fiber-loop ring-down
32 spectroscopy: a sensitive absorption technique for small liquid samples, *Rev. Sci. Instrum.*
33 2003, **74**, 4818–4826.
- 34 [61] Tarsa, P. B.; Wist, A. D.; Rabinowitz, P.; Lehmann, K. K. Single-cell detection by cavity ring-
35 down spectroscopy, *Appl. Phys. Lett.* 2004, **85**, 4523–4525.
- 36 [62] Tarsa, P. B.; Lehmann, K. K. Cavity ring-down biosensing; in Ligler, F. S.; Tait, C. R., editors
37 *Optical Biosensors: Today and Tomorrow*, Second edition; Elsevier: Amsterdam, 2008,
38 pp. 403–418.
- 39 [63] Pipino, A. C. R. Ultrasensitive surface spectroscopy with a miniature optical resonator, *Phys.*
40 *Rev. Lett.* 1999, **83**, 3093–3096.
- 41 [64] Grudinin, I. S.; Ilchenko, V. S.; Maleki, L. Ultrahigh optical Q factors of crystalline resonators in
42 the linear regime, *Phys. Rev. A* 2006, **74**, 063806.
- 43 [65] Johnston, P. S.; Lehmann, K. K. Cavity enhanced absorption spectroscopy using a broadband
44 prism cavity and a supercontinuum source, *Opt. Express* 2008, **16**, 15013–15023.
- 45 [66] Snee, M.; Hannemann, S.; Van Duijn, E. J.; Ubachs, W. Deep-ultraviolet cavity ringdown
46 spectroscopy, *Opt. Lett.* 2004, **29**, 1378–1380.
- [67] Gopalsami, N.; Raptis, A. C.; Meier, J. Millimeter-wave cavity ringdown spectroscopy, *Rev. Sci.*
Instrum. 2002, **73**, 259–262.